

An Experimental Analysis of Visible Light Positioning in NLoS Environments

Sander Bastiaens^{1,†}, Morteza Alijani^{1,*,†}, Wout Joseph^{1,†} and David Plets^{1,†}

¹*Department of Information Technology, imec-WAVES/Ghent University, Technologiepark-Zwijnaarde 126, 9052 Ghent, Belgium*

Abstract

Visible light positioning (VLP) is an emerging and promising technology in the indoor positioning system (IPS) landscape that provides centimeter-level accuracy at a low cost. However, it needs to be more thoroughly investigated, particularly in industrial environments where the presence of metal imposes a significant multipath effect and degrades the VLP accuracy. The absence of literature studies that evaluate VLP in the presence of multipath prompts us to conduct our own set of experiments. The main goal of this paper is to provide insight regarding the spatial extent to which the positioning performance is noticeably affected. Moreover, the effects of shadowing as well as reflections are considered, with the term Non-Line-of-Sight (NLoS) referring to both effects. The experimental results demonstrate that the increase in received light intensity due to reflections depends on the relative location of the light-emitting diode (LED), the photodiode (PD), and the reflecting surface. For the investigated configuration, it is observed that the localization error can be impacted up to 1.5m from a metal closet, with a pronounced specular component. Finally, it is experimentally confirmed that NLoS effects are rather deterministic, which allows them to be modeled.

Keywords

Visible light positioning (VLP), Non-Line-of-Sight (NLoS), Multipath, Shadowing, Experimental analysis

1. Introduction

The indoor location market value is expected to reach \$50.2 billion by 2027 [1] with applications such as discovery, emergency support, and disaster management; business intelligence solutions; information management (e.g., social networks, sports, games, etc.); mapping, navigation, and tracking [1,2]. At the heart of a location-based service (LBS) is a (real-time) location system (RTLS) that accurately and reliably determines the location of a user or an object. Several radio frequency (RF)-based technologies, including radio-frequency identification (RFID), wireless local area network (WLAN), ZigBee, Bluetooth Low Energy (BLE), Ultra-Wideband (UWB), and Ultrasound, have been proposed for indoor positioning system (IPS) [1]. However, they face constraints such as the requirement for costly and dedicated infrastructure, the impact of multipath effects, and, an RF spectrum crunch [2].

Proceedings of the Work-in-Progress Papers at the 13th International Conference on Indoor Positioning and Indoor Navigation (IPIN-WiP 2023), September 25–28, 2023, Nuremberg, Germany

*Corresponding author.

†These authors have the same affiliation.

✉ sander.bastiaens@ugent.be (S. Bastiaens); morteza.aliyani@ugent.be (M. Alijani); wout.joseph@ugent.be (W. Joseph); david.plets@ugent.be (D. Plets)



© 2023 Copyright for this paper by its authors. Use permitted under Creative Commons License Attribution 4.0 International (CC BY 4.0).

 CEUR Workshop Proceedings (CEUR-WS.org)

Visible Light Positioning (VLP), which uses light-emitting diode (LED) light signals, is an emerging technology for the next generation of low-cost indoor positioning systems (IPSs). It has the potential to address some of the limitations of RF-based localization technologies, such as high cost in either use or installation, electromagnetic (EM) interference, privacy violations, and the problem of an increasingly crowded RF spectrum [2]. However, despite the promising advantages of VLP, it is still in its infancy, and several aspects have not been sufficiently researched. VLP, for example, has yet to be studied in an industrial environment with considerable multipath. The dynamically varying industrial or warehouse setting does not present an easy environment for VLP. It requires systems that remain reliable and fully operational even in the presence of positioning-disruptive factors, such as obstructions that provide shadowing or multipath [3].

Research on the evaluation of VLP in the presence of multipath are scarcely found. Xu et al. [4] suggested a three-dimensional positioning technique for indoor visible light communication (VLC) systems that takes into account multipath reflections and concluded that the positioning error is roughly a linear function of the reflection coefficient. In [5], and [6], a VLC-based IPS based on orthogonal frequency division multiplexing (OFDM) is developed to reduce multipath effects and deliver high data rate transmission. Gu et al. [7] proposed a calibration technique to mitigate the influence of multipath reflections. A multipath reflections assessment for an indoor VLP system investigated in [8] concluded that extending the coverage area of the LEDs with an appropriate layout design can reduce the average positioning error.

In this paper, we will investigate experimentally the influence of multipath reflections caused by the presence of a closet and storage racks on VLP performance. In what follows, we provide a description of the measurement configuration and introduce the experimental scenarios in Section 2. In Section 3, the propagation model and localization approach for our case study will be presented. Section 4, discusses the performance of VLP in NLoS environments based on the obtained results. Finally, conclusions and future works are discussed in Section 5.

2. Experimental Set-up

2.1. Materials and Configuration

2.1.1. Lab Environment

To evaluate VLP system's positioning accuracy, a 4m x 4m x 5m lab was used, whose outskirts are covered with black cloths to minimise external light and uncontrolled reflections. Fig.1 shows the lab and its features. Its inside houses a height-adjustable platform of cable trays, from which various configurations of LED transmitters can be suspended. Below, the wooden floor is strategically perforated to form a uniform square grid with a 0.5 m spacing. The holes' purpose is to accommodate the measuring platform.

2.1.2. LED Transmitter Hardware

Various LED transmitter configurations are at one's disposal. In this work, with reproducibility in mind, most often a combination of commercial components is used. The COB LEDs used in the experiments are of the Bridgelux BXRE-50C3001-D-24 type, having a Lambertian radiation

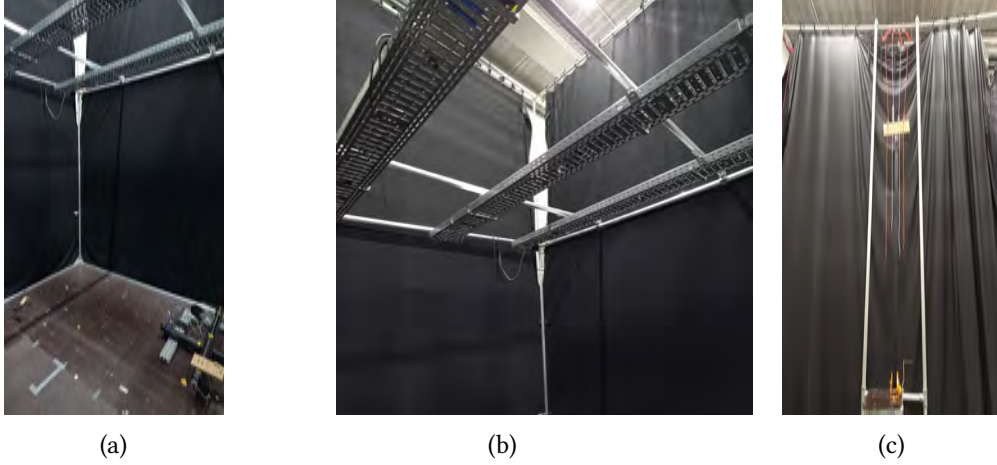


Figure 1: Photographs of the realized VLP lab inside (a), height-adjustable LED mounting system (b), and outside view with LED mounting system (c).

pattern. Experiments are also performed with linear LEDs not having non-Lambertian radiation patterns, namely ETAP's E4010/LED1N060D LEDs. Additionally, both of the employed LED types are intensity modulated to transmit 50% duty cycle square waves with frequencies $f_{c,i} = 2^{i-1} f_0$, ($i = 1, 2, \dots, N$). f_0 is set to 500 Hz to exceed the flicker threshold [11].

Table 1
TX and RX configurations in experiments

Name of Experiment	Transmitter (Tx)	Receiver (RX)	
	LED's Type\Driver \Installing Height	DAQ: Ns[-] /Fs[kHz]	PD's Type/ Gain
Right Corner Rack	BXRE-50C3001-D-24 \LTM8005 Demo Board \4m	5120/256	PDA36A2/40dB
Centre Rack	BXRE-50C3001-D-24 \LTM8005 Demo Board \4m	5120/256	PDA100A2/40dB
Closet with COBs	BXRE-50C3001-D-24 \3m	1500/75	PDA36A2/30dB
Closet with LED armatures	E4010/LED1N060D \4m	1500/75	PDA36A2/40dB

2.1.3. Receiving Hardware

To ensure scientific reproducibility, the default receiver resorts to commercially available devices. It couples a Thorlabs amplified photodetector module with tunable gain, namely the PDA36A2 or PDA100A2 with an active area of $A_R = 13 \text{ mm}^2$ and $A_R = 75.4 \text{ mm}^2$, respectively, to a National Instruments USB-6212 for data acquisition (DAQ). The optical receiver under test is fitted on top of a 2D slider system consisting of motor-Driven Velmex' BiSlides[®] (See Fig.2

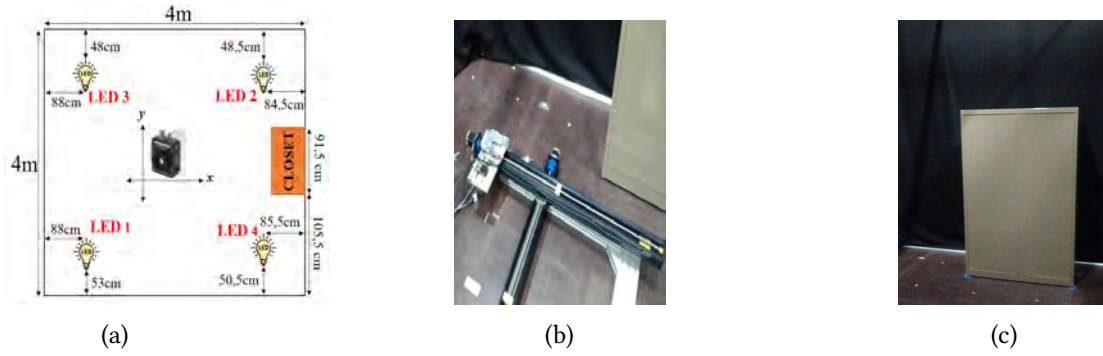


Figure 2: Visualisation of (a) the LED and obstacle distribution in the measurement environment, (b) the slider system part of the measurement setup, and of (c) the metallic closet.



Figure 3: Photographs of the storage racks' (a) front and (b)-(d) backside. The latter keeps (b) the whole rack, (c) the left half, and (d) the right half in view, respectively.

(b)). This measurement system covers a 1m by 1m zone with a predefined (here mostly 2.5 cm) granularity and a submillimetre accuracy. By sequentially displacing it, for which the alignment is ensured by the holes in the floor, the complete 4m x 4m receiver plane can be traversed. A MATLAB® (or Python) backend is responsible for addressing the sliders, the sensor read-out, and the data manipulation.

2.2. Experimental Scenarios

To investigate the NLoS influence on the VLP performance, we used both a greige-green lacquered metallic closet and storage racks with carton boxes as typical obstacles in our experimental measurements, depicted in Fig.2 (c) and Fig.3 (a-d), respectively. To induce more homogeneous reflections, the closet is turned with its backside to the positioning area (See Fig.2 (c)). The arrangement of each experiment is shown in Table.1.

3. Propagation Model and Localization

3.1. Channel Model

As the area is confined by black cloths, we assume the receiving photodiode (PD) will receive light either along the Line-of-Sight (LoS) path or along a first-order reflection off the closet or rack. Fig.4 shows how the optical light channel is usually modeled in the case of NLoS

radiation pattern, and it is typically governed by Phong's model consisting of both diffuse and specular parts [12]. It should be noted that the NLoS components are the same LoS variables with the symbol prime '. The PD generates photocurrent contributions $I_{PD,i}$ in response to incident light and the measured $P_{R,i}$ values are linked to $I_{PD,i}$ using the nominal responsivity \widehat{R}_P of the photodiode as follows [11]:

$$P_{R,i} = \frac{I_{PD,i}}{M \cdot \widehat{R}_P} \quad (5)$$

where M is defined as a gain mismatch factor. It accounts for the wavelength λ mismatch between transmitter and receiver [11].

3.2. Localization Measurement Set-up

For localization and measuring $I_{PD,i}$, the LED i 's photocurrent magnitude-based RSS (received signal strength) values, we installed the PDA36A2 or PDA100A2 on top of the 2D slider system. Moreover, 15 $I_{PD,i}$ values are averaged per measurement location to minimize the noise impact. For demultiplexing the contributions of the different LEDs, we employed the Fast Fourier Transform (FFT)-based demodulation as presented in [11]. Next, after deriving the set of RSS values, we used model-based fingerprinting (MBF) for localization, only accounting for the LoS contribution, which means that MBF depends on a propagation model that only assumes LoS propagation without considering any reflections [9]. Notice that the model is based on a propagation model, and not on actually measuring/fingerprinting the area experimentally. The estimated location in the utilized approach is the location having the lowest sum of squared differences between measured and modeled received powers. Finally, positioning error is defined as the 2D Euclidean distance between the estimated and actual ground truth locations.

4. Experimental Results and Discussion

4.1. Uniform Closet

Fig.5 depicts the 4 LEDs' $I_{PD,i}$ planar distributions, obtained with the PDA36A2 in the presence of the closet. From Fig.5 (a)-(d), it is clear that due to light's particle/ray (dual) nature NLoS effects are much more deterministic, and hence predictable for VLP than for sub-GHz radio frequency signals. Shadowing locally effectuates a large $I_{PD,i}$ reduction. In Fig.6 (a), it is visualised by the cluster of points with an $I_{PD,i}$ that is smaller than what it would be in LoS conditions. With light the $I_{PD,i}$ magnitude originating from diffraction is limited. It effectuates that in the shadow areas $I_{PD,i}$ nears the noise floor. Moreover, multipath's $I_{PD,i}$ enlarging contribution (i) depends on the relative positioning of the LED and the closet through the irradiance angle during reflection θ_i , (ii) is spatially confined to around a 1.5m vicinity of the closet, and (iii) exhibits a pronounced specular component. Furthermore, differentiating LED 2 and 3's $d_i - I_{PD,i}$ curves of Fig.6 (a)/(b) shows both that the $I_{PD,i}$ of the LEDs closer to the obstacle are relatively larger affected, and that the multipath contribution can be of significant magnitude. From a trilateration point-of-view, the obstacle-induced $I_{PD,i}$ surplus

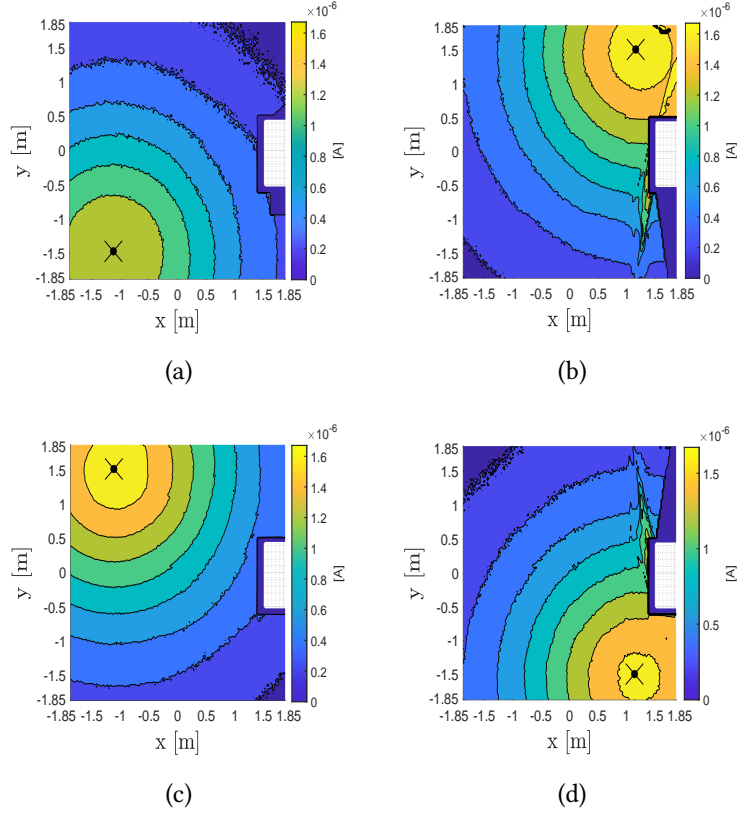


Figure 5: Distribution of $I_{PD,i}$ for (a) LED 1, (b) LED 2, (c) LED 3 and (d) LED 4 (Fig.2(a)) in the presence of the matte metallic closet's backside. In each plot, the black marker represents the considered LED's location.

entails an underestimating of the inter-LED-PD distance. This underestimation, and $d_i - I_{PD,i}$'s noninvertibility in general, will impede highly-accurate localisation around the obstacle.

Fig.7 quantifies the spatial extent of the impact of closet-induced multipath on the 2D positioning performance. The NLoS influence mainly manifests locally around the obstacle, and specifically around the specular reflection vector of each of the LEDs. Expectedly, positioning outliers are found in the regions of $I_{PD,i}$ surplus. These do not exceed the 1m error bound. Moreover, all in all, MBF copes well when a single LoS link obstruction occurs. The errors in the left top and bottom corners are mainly the result of the $P_{t,i}$ (the radiant flux of LED i) calibration of LEDs 2 and 4, which did not correct their NLoS contribution. Typically, this $P_{t,i}$ calibration would be performed beforehand and in controlled circumstances. Finally, Fig.8 demonstrates that the obstacle-induced NLoS is also dependent on the LED fixture's nature. It shows the $I_{PD,2}$ and $I_{PD,4}$ distribution in the presence of ETAP's E4010/LED1N060D. Similarly, as for the COB LED case, a strong RSS reduction due to shadowing is observed, as well as an increased RSS due to closet-induced specular reflections. Notice that, due to practical constraints, we were unable to measure right up to the closet, leaving some space. This is especially visible in Fig.8, and we should not interpret it as shadows.

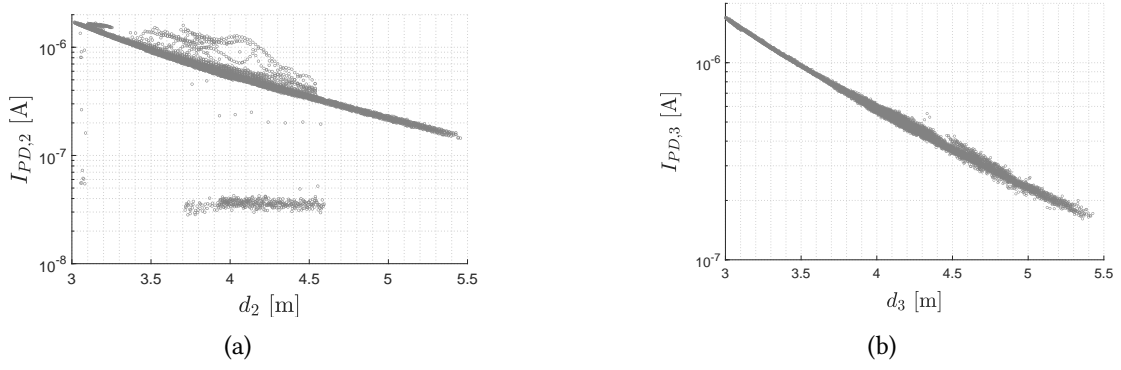


Figure 6: A representation of (a) LED 2's and (b) LED 3's $d_i - I_{PD,i}$ data in graph format in the experiment closet with COBs.

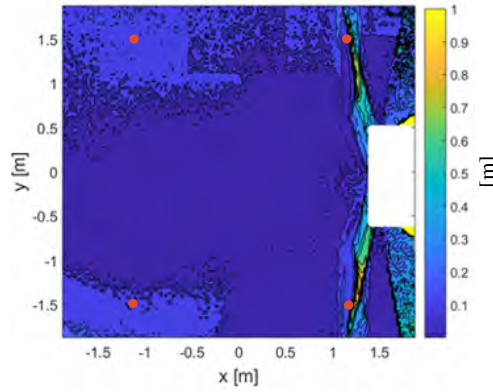


Figure 7: The spatial distribution of MBF's positioning error in the closet configuration with LED armatures. The LED locations are represented in red.

Additionally, we employed the Rician K-factor (K_r) to visualize the NLoS contribution in our experiment. K_r is defined as the ratio between the LoS power (P_{LoS}), determined via an identical measurement without a closet, and the power in all other scattered paths (P_{NLoS}), determined as the power in the closet scenario minus the power in the without-closet scenario, $K_r = 10 \log_{10} \left(\frac{P_{LoS}}{P_{NLoS}} \right) (dB)$ [13]. Notice that as this approach for determining the LoS and NLoS contributions is only valid when the received power in the no-closet scenario is smaller than or equal to the received power in the closet scenario, we here exclude the areas that are shadowed by the closet. The grey areas in Fig.9, therefore, indicate the shadowed areas (as well as the areas right next to the closet where measurements were practically impossible). Figs.9 (a) and (b) show K_r for LED2 (top right LED) and LED4 (bottom right LED), respectively. From both figures, K_r generally drops when moving away from the LED. In Figs.9 (a) and (b), zones C indicates that further away from the LEDs, the NLoS contribution falls within the noise floor, while the LoS contribution decreases with distance. The highlighted areas of A and B, on the other hand, illustrate that there has been a sharp drop in the K_r because of the larger contributions of NLoS due to the closet.

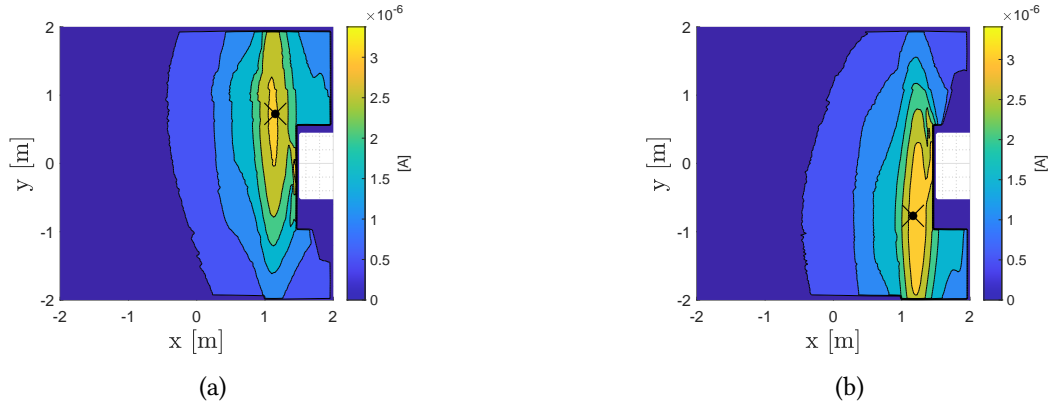


Figure 8: The $I_{PD,i}$ distribution for (a) LED 2 and (b) LED 4, when employing the non-Lambertian E4010/LED1N060D LEDs (Experiment closet with LED armatures).

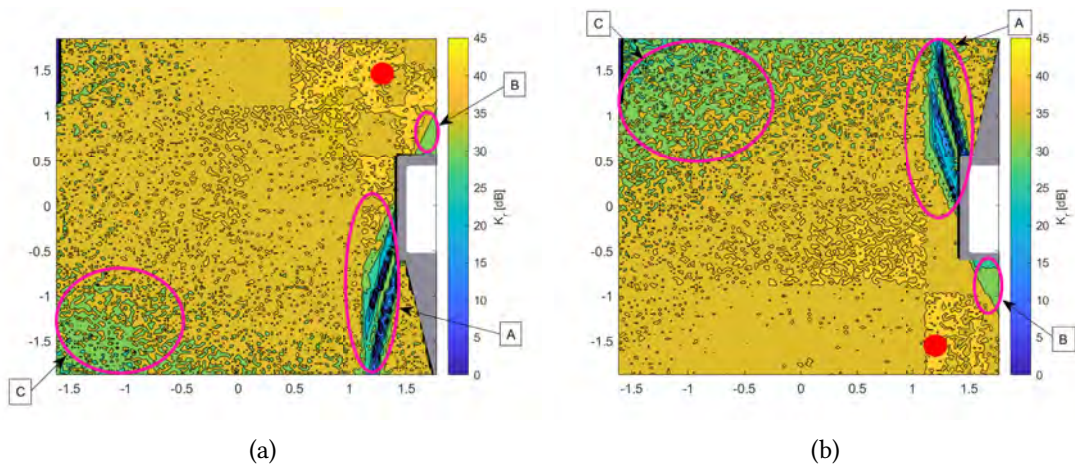


Figure 9: K_r in the presence of (a) LED 2 and (b) LED 4. The LED location is indicated in red.

4.2. Storage Rack

To provide insight into the expected NLoS extent encountered during industrial deployments, Fig.3's imaged storage rack features in two configurations. Fig.10 shows the $I_{PD,i}$ found when the storage rack is located at the outside of the positioning zone, while Fig.11 does so for a scenario in which the storage rack is located in between the LED arrangement. Fig.10 and Fig.11 display the more complex multipath and obstruction nature of the storage rack. It is a consequence of the heterogeneity of the storage rack (and its contents). The narrow, highly-reflective metal structures introduce very directive $I_{PD,i}$ contributions, as can be remarked from Fig.10 (c) and (e) for instance. Luckily, the associated influence on the positioning is spatially confined as well. The accuracy diminishing effect of the first storage rack configuration is treated by Almadani et al. in [3]. The more irregular shadowing pattern is particularly discernible around the tangent of the LED and the far storage rack corner that is in view. There, one of two neighbouring grid points can be shadowed, while the other features in LoS. For example, when

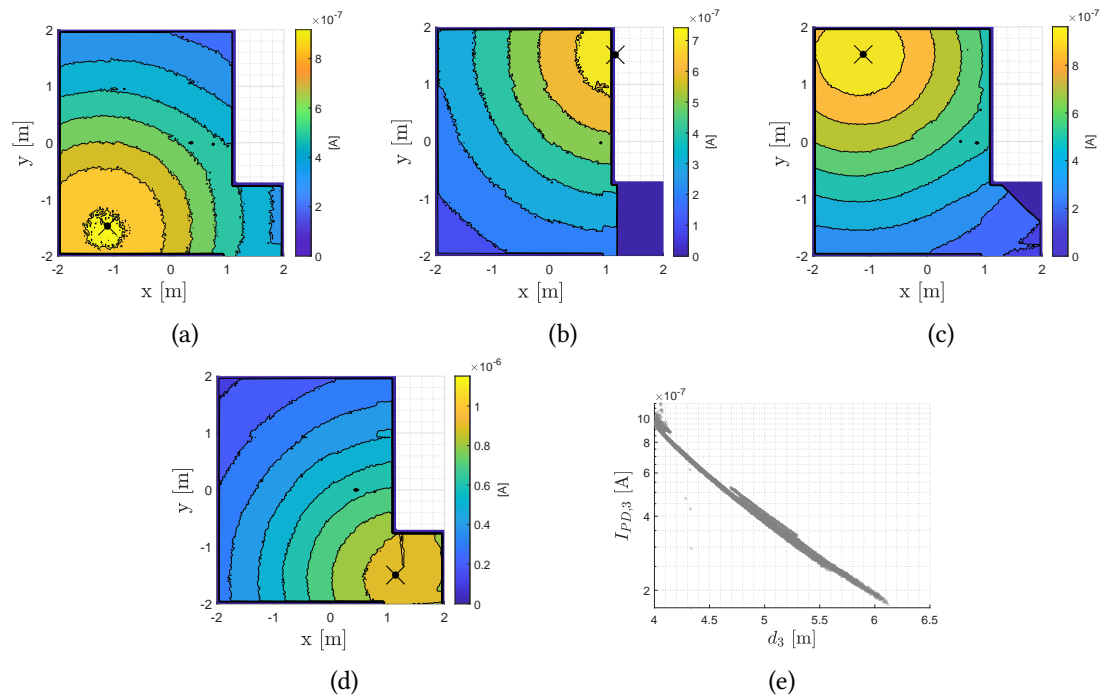


Figure 10: $I_{PD,i}$ distribution of (a)-(d) LEDs 1-4 (in order) for the first storage rack configuration (top corner right). $d_3 - I_{PD,3}$ is depicted in (e).

the points are located more towards the negative y-coordinates than the storage rack is, the former's light is blocked by, while the latter's propagates between, the metallic structures. A final remark constitutes that to guarantee a sufficient amount of LoS links in the presence of closely spaced rows of tall storage racks, the exact location and shape of obstacles are needed for VLP with a fine granularity, which for RF is not the case for example [2]. In addition, Fig. 12 (a) and (b) show besides the LoS (upper cluster) and the shadow (lower cluster) characteristic, also grid points whose main contributions are of diffracted (and thus attenuated) light. To sum up, the NLoS influence of VLP should be much more predictable and spatially-confined than is the case for RF-based IPS. This would mean that well-characterised and fixed obstacles could be accounted for, e.g. by incorporating it in MBF's propagation map. This approach requires an accurate representation model of the real-life propagation. The aptitude of propagation model, in conjunction with Phong reflections, in describing VLP reflections is still to be proven [2]. Unfortunately, most industrial environments being dynamically-varying, sporting a mobile and heterogeneous obstacle distribution, renders such an approach difficult to realise in practice. Importantly, on the basis of these experiments, in industrial deployments with sparse obstacles, mostly local positioning outliers are expected. Moreover, these outliers would then be confined to the area near the obstacles, which is one that is frequently avoided with vehicular assets. For example, for safety reasons, if possible, an Automated Guided Vehicle (AGV) will not be required to drive past a storage rack with a significant velocity, without having at least a 20 cm margin [2].

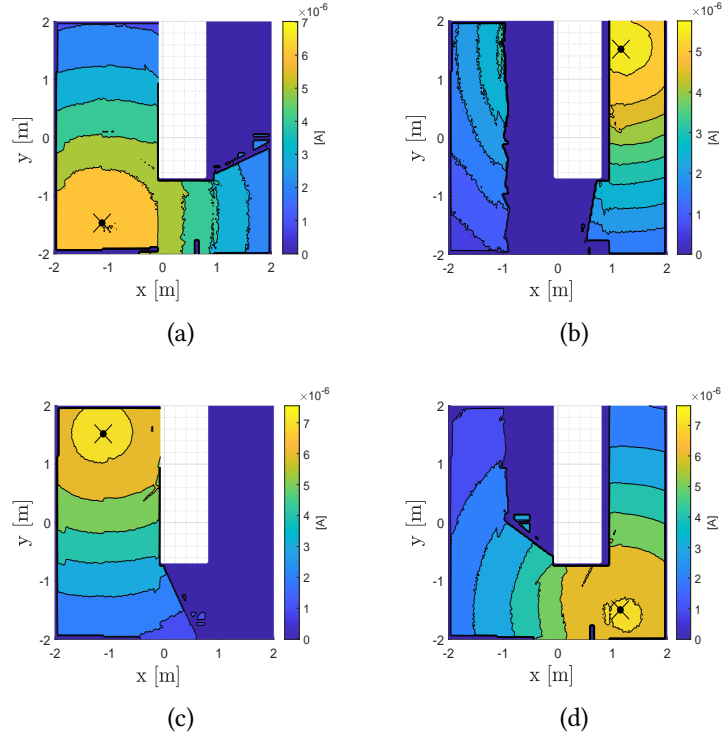


Figure 11: $I_{PD,i}$ distribution of (a)-(d) LEDs 1-4 (in order) for the second storage rack configuration (top near to centre). A measurement error occurred at the figures' bottom near the centre.

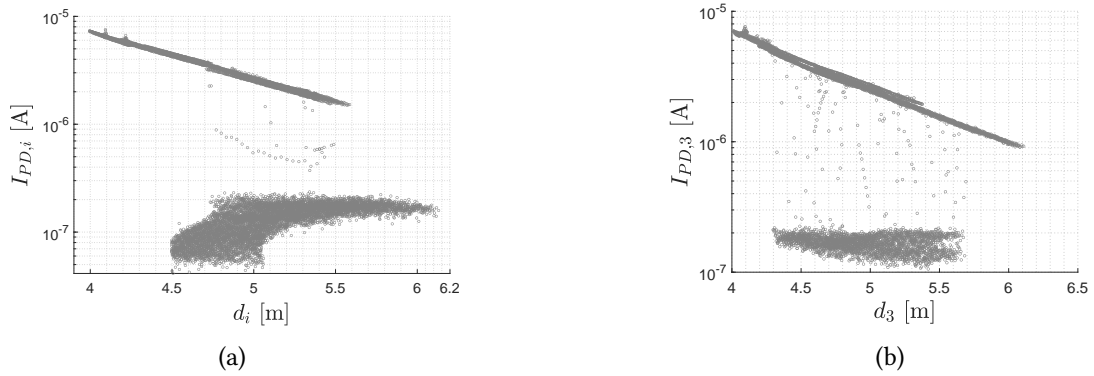


Figure 12: A representation of the $d_i - I_{PD,i}$ line graph of LED2 and LED3, respectively, in the experiment centre rack.

5. Conclusion

This paper conducts an experimental investigation into the accuracy of VLP in environments with induced obstacles, such as metallic closet and storage racks. Two VLP's accuracy degradation factors, including multipath and shadowing, are considered, which are both collectively

referred to as NLoS impacts. The experimental results demonstrate that the obstacle-induced NLoS influences (i) are much more deterministic and therefore predictable for VLP than for the sub-GHz radio frequency (RF) signals, (ii) are vastly dependent on the local deployment of the LED transmitters and the location of the obstacles through the irradiance angle during reflection, (iii) are spatially confined to around a 1.5m vicinity of the obstacles because of attenuation due to high path loss, and finally (iv) are dependent on the nature of the LED fixture. Future work could include experimental modelling of the NLoS contributions and incorporating these into MBF-based localization approaches to mitigate NLoS-induced positioning errors.

References

- [1] URL: <https://www.researchandmarkets.com/reports/5135900/global-location-based-services-lbs-and-real#tag-pos-1>
- [2] S. Bastiaens, Towards centimetre-order indoor localisation with RSS-based visible light positioning, Ghent University. Faculty of Engineering and Architecture, Ghent, Belgium, 2022.
- [3] Y. Almadani, M. Ijaz, B. Adebisi, S. Rajbhandari, S. Bastiaens, W. Joseph, D. Plets, An experimental evaluation of a 3D visible light positioning system in an industrial environment with receiver tilt and multipath reflections, in: *Optics Communications*, vol. 483, no. 126654, 2021, pp. 1–11. doi: 10.1016/j.optcom.2020.126654.
- [4] J. Xu, H. Shen, W. Xu, H. Zhang, X. You, LED-Assisted Three-Dimensional Indoor Positioning for Multiphotodiode Device Interfered by Multipath Reflections, in: Proceedings of the 2017 IEEE 85th Vehicular Technology Conference (VTC Spring), Sydney, NSW, Australia, 2017, pp. 1-6. doi: 10.1109/VTCspring.2017.8108349.
- [5] M. Aminikashani, W. J. Gu, M. Kavehrad, Indoor Location Estimation with Optical-based OFDM Communications, URL: <https://arxiv.org/pdf/1506.07571.pdf>
- [6] M. Aminikashani, W. J. Gu, M. Kavehrad, Indoor Positioning in High Speed OFDM Visible Light Communications, URL: <https://arxiv.org/pdf/1505.01811.pdf>
- [7] W. Gu, M. Aminikashani, P. Deng, M. Kavehrad, Impact of Multipath Reflections on the Performance of Indoor Visible Light Positioning Systems, in: *Journal of Lightwave Technology*, vol. 34, no. 10, May 15, 2016, pp. 2578-2587. doi: 10.1109/JLT.2016.2541659.
- [8] W. Gu, M. A. Kashani, M. Kavehrad, Multipath Reflections Analysis on Indoor Visible Light Positioning System, URL: <https://arxiv.org/pdf/1504.01192.pdf>
- [9] D. Plets, A. Eryildirim, S. Bastiaens, N. Stevens, L. Martens, W. Joseph, A Performance Comparison of Different Cost Functions for RSS-Based Visible Light Positioning Under the Presence of Reflections, in: *Proceedings of the 4th ACM Workshop on Visible Light Communication Systems (VLCS)*, Snowbird, Utah, USA, Oct. 16, 2017, pp. 37–41. doi: 10.1145/3129881.3129888.
- [10] T. Komine, M. Nakagawa, Fundamental analysis for visible-light communication system using LED lights, in: *IEEE Transactions on Consumer Electronics*, vol. 50, no. 1, Feb. 2004, pp. 100-107. doi: 10.1109/TCE.2004.1277847.
- [11] S. Bastiaens, W. Raes, N. Stevens, L. Martens, W. Joseph, D. Plets, Impact of a Photodiode's

- Angular Characteristics on RSS-Based VLP Accuracy, in: IEEE Access, vol. 8, 2020, pp. 83116-83130. doi: 10.1109/ACCESS.2020.2991298.
- [12] C.R. Lomba, R.T. Valadas, A.M. de Oliveira Duarte, Experimental characterisation and modelling of the reflection of infrared signals on indoor surfaces, in: IEE Proceedings - Optoelectronics, vol. 145, no.3, 1998, pp. 191 – 197. DOI: 10.1049/ip-opt:19982020.
- [13] C. Tepedelenlioglu, A. Abdi, G. B. Giannakis, The Ricean K factor: estimation and performance analysis, in: IEEE Transactions on Wireless Communications, vol. 2, no. 4, July 2003, pp. 799-810. doi: 10.1109/TWC.2003.814338.